Mode conversion of acoustic phonons by a superlattice with isotropic layers

Hatsuyoshi KATO

(Received on 28 November 1997)

Tomakomai National College of Technology
Nishikioka,Tomakomai 059-1275, Japan

A fundamental idea of mode converter of acoustic phonons is proposed. The idea is based on the resonant condition of transmission of acoustic phonons in a superlattice. At this condition, the wave energy oscillates back and forth between the two acoustic modes while the phonons get through the superlattice. This effect is analyzed in terms of the transfer matrix method and finite difference equations. Mechanism of the mode conversion is analogous to the MSW effect in the field of neutrino physics, and the structure of the mode converter have the feature of a CHIRP (coherent hetero-interfaces for reflection and penetration) superlattice.

I. INTRODUCTION

Recently, we have reported an unusual behavior of the transmission and reflection characteristic of phonons in a superlattice (SL) at an oblique angle of propagation.[1] Specifically, for frequencies in the vicinity of anti-crossing frequency in the SL dispersion relation, the wave energy oscillates back and forth between the different polarizations as the wave propagates through the SL. These oscillations are analogous to the Pendellösung effect for electrons and to the Borrmann effect (the anomalous transmission effect) for X-rays.[2,3]

When X-rays, for instance, are incident to a very perfect crystal with a certain angle, there are strong reflected beam and simultaneously a strong transmitted beam of about equal intensities in spite of an absorption characteristic of the crystal.[3] In the case of phonons in SLs, the reflected and transmitted beams correspond to the different acoustic phonon modes, i.e., transverse (T) and longitudinal (L) and the acoustic energy of the mode converted from the incident polarization steadily grows. This effect is also analogous to the oscillations in neutrino physics, which are predicted to occur between different neutrino flavors if neutrinos have mass.

When neutrinos with definite energy propagate through matter with varying electron density rather than through free space, an interesting additional effect referred to as the Mikheyev-Smirnov-Wolfenstein (MSW) effect [4,5] occurs. More explicitly, the resonant amplification of oscillations or an almost complete conversion of one neutrino flavor into the other should take place. A similar effect is expected to occur for the case of phonons which propagate through a SL with varying thickness of bilayers. In the present work we study this effect for phonons in SLs.

Figure 1 (a) shows a SL consisting of three sub-superlattices (i.e. SL1, SL2, SL3) alternated thin elastic *single-layers* of two different materials. In each sub-SL, the single-layer thicknesses, D_A and D_B, are assumed to be common to both A and B. The structure of a *bi-layar* (BL) is depicted in Fig.1(b). However the D_A and D_B are slightly incremented (or decremented), i.e., SL1 has thickness of BLs thinner than that of SL2, and SL3 has BLs thicker than SL2. This type of SL is analogous to CHIRP (coherent hetero-interfaces for reflection and penetration) superlattices which has many attractive features for device application.[6]

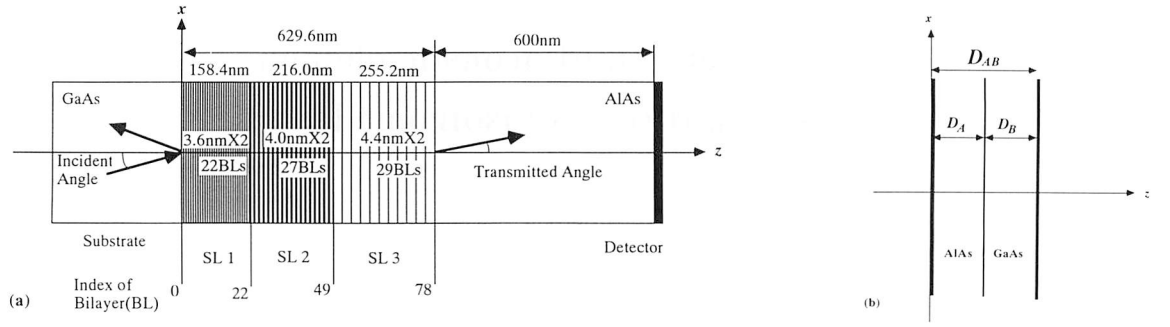

Fig.1. Schematic geometry of the superlattice structure is depicted. Each layer is assumed to be made from amorphous GaAs or AlAs, as well as substrate and a 600nm buffering region. (a) The thickness of each constituent *single-layar* in a *bi-layar* (BL) of sub-SLs is incremented by step wise. At the center of the SL (SL2), the BL satisfies the resonant condition of transmission. The substrate and detector are assumed to have the elastic properties of B and A layers, respectively. (b) The structure of BLs in each sub-SL is the same and each single-layer has thickness either D_A or D_B. Total thickness of a BL then becomes $D_A + D_B = D_{AB}$.

In Sec.Ⅱ, the transfer-matrix method is introduced and we get an approximated 2×2 transfer matrix which relates the phonon amplitudes of adjacent BLs. In Sec.Ⅲ, finite difference equations which relates the phonon amplitudes in the adjacent BLs are derived and they are solved. From this results, we propose a fundamental idea for the mode converter or selector in Sec.Ⅳ.Numerical examples for the conversion rates are given in Sec.Ⅴ, and we show the mode converter also plays a role of mode selector of the acoustic phonons. Section Ⅵ summarizes the present work.

Ⅱ. TRANSFER MATRIX

We consider the coupled transverse and longitudinal vibrations and write the displacement vector in a single-layer as follows:

$$\mathbf{u}_n^{(j)} = \sum_{J=\mathrm{T,L}} \{ a_{J,n}^{(j)}\, \mathbf{e}^{(j)} \exp(ik^{(j)} z_n^{(j)}) + b_{J,n}^{(j)}\, \tilde{\mathbf{e}}^{(j)} \exp(-ik^{(j)} z_n^{(j)}) \}\, e^{ik_{\parallel} x - i\omega t}, \quad (j=A,B), \tag{1}$$

where n indicates an index of BL in the SL, j discriminates the constituent materials A and B in Fig.1(b); $a_{J,n}^{(j)}$ and $b_{J,n}^{(j)}$ are the amplitudes of the transmitted and reflected phonons of mode J, respectively; $\mathbf{e}^{(j)}$ and $\tilde{\mathbf{e}}^{(j)}$ are the unit polarization vectors; $k_{\parallel}$ and $k^{(j)}$ are the wave numbers parallel and perpendicular to the interfaces, respectively.

The transfer-matrix method is a useful way to obtain the transmission and reflection rates of phonons in SLs. For SLs consisting of crystalline layers with elastic anisotropy, the relevant transfer matrix is a 6×6 matrix, in general. In the present case, however, the transfer matrix is a 4×4 matrix because we consider isotropic elastic media. The phonon amplitudes $a_{J,n+1}^{(j)}$ and $b_{J,n+1}^{(j)}$ in a BL is related to the ones in the previous BL $a_{J,n}^{(j)}$ and $b_{J,n}^{(j)}$ by multiplication with a transfer matrix.[7] Thus

$$\begin{pmatrix} a_{T,n+1}^{(j)} \\ a_{L,n+1}^{(j)} \\ b_{T,n+1}^{(j)} \\ b_{L,n+1}^{(j)} \end{pmatrix} = \mathrm{F}_n^{(j)} \begin{pmatrix} a_{T,n}^{(j)} \\ a_{L,n}^{(j)} \\ b_{T,n}^{(j)} \\ b_{L,n}^{(j)} \end{pmatrix}, \tag{2}$$

where the transfer matrix $F_n^{(j)}$ is given by

$$F_n^{(j)} = \Phi_n^{(j)}\, f^{(kj)}\, \Phi_n^{(k)}\, f^{(jk)}, \tag{3}$$

$$(j=A \text{ and } k=B, \text{ or } j=B \text{ and } k=A),$$

$$\Phi_n^{(j)} = \begin{pmatrix} \exp(ik_T^{(j)} D_n^{(j)}) & 0 & 0 & 0 \\ 0 & \exp(ik_L^{(j)} D_n^{(j)}) & 0 & 0 \\ 0 & 0 & \exp(-ik_T^{(j)} D_n^{(j)}) & 0 \\ 0 & 0 & 0 & \exp(-ik_L^{(j)} D_n^{(j)}) \end{pmatrix} \tag{4}$$

$$f^{(jk)} = \left[M^{(k)} \right]^{-1} M^{(j)}, \tag{5}$$

$$M^{(j)}=\begin{bmatrix} \cos\phi_T & \sin\phi_L & -\cos\phi_T & \sin\phi_L \\ -\sin\phi_T & \cos\phi_L & -\sin\phi_T & -\cos\phi_L \\ c_{44}\dfrac{\cos 2\phi_T}{\sin\phi_T} & 2c_{44}\cos\phi_L & c_{44}\dfrac{\cos 2\phi_T}{\sin\phi_T} & -2c_{44}\cos\phi_L \\ -2c_{44}\cos\phi_T & c_{44}\sin\phi_L\dfrac{\cos 2\phi_T}{\sin^2\phi_T} & 2c_{44}\cos\phi_T & c_{44}\sin\phi_L\dfrac{\cos 2\phi_T}{\sin^2\phi_T} \end{bmatrix} \tag{6}$$

In these expressions $D_n^{(j)}$ is the thickness of the layer j in the nth BL. The matrix $\Phi_n^{(j)}$ represents the associated phase change for phonons, ϕ_J is the angle of incidence or reflection of the phonon mode J; c_{44} is the stiffness coefficient. On the r.h.s. of Eq.(6), we have omitted the superscript j from ϕ_T, ϕ_L and c_{44}, for simplicity. In each sub-SL of Fig.1 (a), $D_n^{(j)}$'s do not depend on the index n of BL, and they are expressed as D_A and D_B as in Fig.1 (b). Further, $F_n^{(j)}$ and $\Phi_n^{(j)}$ do not depend on n if we consider periodic SLs. From Eq.(5), we note that the matrix $f^{(jk)}$ satisfies

$$f^{(kj)}=\left[f^{(jk)}\right]^{-1}. \tag{7}$$

This matrix consists of the amplitudes transmission and reflection coefficients at a single interface for a phonon incident to j layer from k layer.

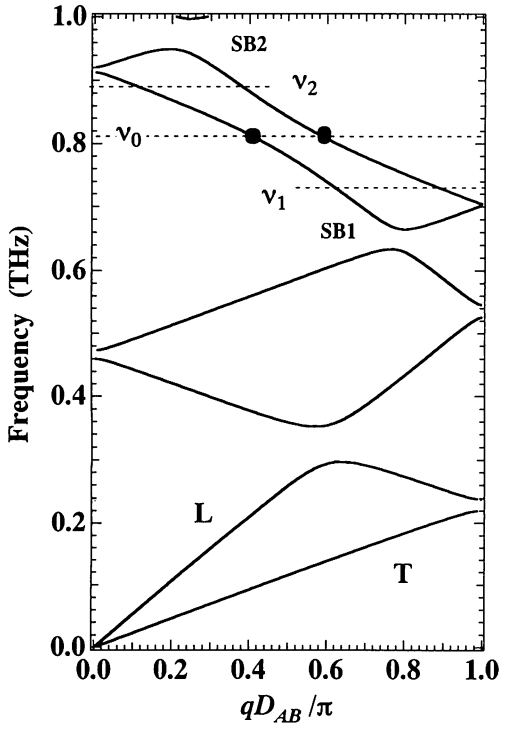

Fig.2. Phonon dispersion relations in a periodic GaAs/AlAs superlattice in the isotropic, continuum approximation. The thicknesses of A layer (AlAs) D_A and B layer (GaAs) D_B are the same as 4.0nm; the periodicity is $D_{AB} = D_A + D_B = 8.0$nm. Therefore, this is a dispersion relation for SL2. The lowest anticrossing frequency is denoted by $\nu_0 = 812$GHz. The other sub-SLs, SL1 and SL3, have similar dispersion relations. Equivalent frequency for SL1 in this figure is $\nu_1 = 731$GHz, that of SL3 is $\nu_2 = 893$GHz. The propagation direction is such that the direction of the L (T) mode is 45°(25.2°) in the GaAs layers and 57.5°(30.5°) in the AlAs layers, respectively.

Making use of the 4 × 4 matrices discussed above, we can get a dispersion relation as in Fig.2. It is depicted for the SL2 that has BLs to satisfy the resonant condition of transmission with frequency $\nu_0 = 812$GHz.[1] Incident angle is $\phi_L^{(B)} = 45°$ ($\phi_T^{(B)} = 25.2°$). The branches near the frequency ν_0 have the anti-crossing feature. (See Sec. Ⅳ for the meaning of frequencies ν_1 and ν_2.)

The formulation based on the 4 × 4 transfer matrix given above is still intractable for the analytical calculations. Accordingly, we develop an approximated formula for the transmission of phonons which utilizes the matrices of 2 × 2. The amplitudes we keep here are only those of transmitted phonons, i.e., a_T and a_L. Thus, equations (3) and (4) become for $j = B$ and $k = A$ (hereafter we omit the superscript for the 2 × 2 transfer matrix $\hat{F}$),

$$\hat{F}_n=\hat{\Phi}_n^{(B)}\,\hat{f}^{(AB)}\,\hat{\Phi}^{(A)}\,\hat{f}^{(BA)}, \tag{8}$$

$$\hat{\Phi}_n^{(j)}=\begin{bmatrix} \exp(ik_T^{(j)}D_n^{(j)}) & 0 \\ 0 & \exp(ik_L^{(j)}D_n^{(j)}) \end{bmatrix}, \tag{9}$$

where

$$\hat{f}^{(jk)}=\begin{bmatrix} [f^{(jk)}]_{11} & [f^{(jk)}]_{12} \\ [f^{(jk)}]_{21} & [f^{(jk)}]_{22} \end{bmatrix}. \tag{10}$$

In this approximation, we should note that the 2 × 2 matrix $\hat{f}^{(jk)}$ consists of the elements of the 4 × 4 matrix $f^{(jk)}$, but is not defined by Eq.(10) with matrices M simply reduced to 2 × 2. This means we neglect the amplitude reflection coefficients, but not the reflected amplitude $b_{j,n}^{(j)}$. This approximation is valid in frequencies near the resonant condition of transmission because reflection from interfaces of the SL is strongly suppressed. (See Fig.5 (a)) A crucial

point is that we require the same relation as Eq.(7) holds for the reduced matrix $\hat{f}^{(jk)}$, i.e.,

$$\hat{f}^{(kj)}=\left[\hat{f}^{(jk)}\right]^{-1}, \tag{11}$$

or this equation defines $\hat{f}^{(kj)}$.

With these matrices, Eq.(2) is reduced to

$$\begin{bmatrix} a_{T,n+1} \\ a_{L,n+1} \end{bmatrix}=\hat{F}_n \begin{bmatrix} a_{T,n} \\ a_{L,n} \end{bmatrix}, \tag{12}$$

where the amplitudes $a_{T,n}$ and $a_{L,n}$ are those in the B layer (we also omit the superscripts of $a_{T,n}$ and $a_{L,n}$, hereafter).

Ⅲ. FINITE DIFFERENCE EQUATIONS

In order to find equations satisfied by the transmitted amplitudes of T and L phonons we need an additional equation which relates the amplitudes $a_{J,n+2}$ with $a_{J,n+1}$, i.e.,

$$\begin{bmatrix} a_{T,n+2} \\ a_{L,n+2} \end{bmatrix}=\hat{F}_{n+1} \begin{bmatrix} a_{T,n+1} \\ a_{L,n+1} \end{bmatrix}, \tag{13}$$

where $\hat{F}_{n+1}$ is also the transfer matrix for $(n+1)$ th BL defined like $\hat{F}_n$. Using Eqs.(12) and (13), we obtain two difference equations satisfied by the amplitudes of both modes:

$$a_{T,n+2}-\left(\hat{F}'_{11}+\hat{F}_{22}\frac{\hat{F}'_{12}}{\hat{F}_{12}}\right)a_{T,n+1} +\left(\hat{F}_{11}\hat{F}_{22}\frac{\hat{F}'_{12}}{\hat{F}_{12}}-\hat{F}'_{12}\hat{F}_{21}\right)a_{T,n}=0, \tag{14a}$$

$$a_{L,n+2}-\left(\hat{F}_{11}\frac{\hat{F}'_{21}}{\hat{F}_{21}}-\hat{F}'_{22}\right)a_{L,n+1} +\left(\hat{F}_{11}\hat{F}_{22}\frac{\hat{F}'_{21}}{\hat{F}_{21}}-\hat{F}_{12}\hat{F}'_{21}\right)a_{L,n}=0, \tag{14b}$$

where $\hat{F}_{jk}$ is a component of the matrix $\hat{F}_n$ and $\hat{F}'_{jk}$ is of $\hat{F}_{n+1}$.

In each sub-SL, $\hat{F}_{jk}=\hat{F}'_{jk}$ Therefore, Eq.(14) is reduced to

$$a_{n+2}-2\tau a_{n+1}+\delta a_n=0, \tag{15}$$

where a_n expresses either $a_{L,n}$ or $a_{T,n}$; and

$$\delta=\det[\hat{F}]$$

$$=\exp(ik_{Tz}^{(A)}D_A+ik_{Tz}^{(B)}D_B+ik_{Lz}^{(A)}D_A+ik_{Lz}^{(B)}D_B), \tag{16}$$

$$\tau=\frac{1}{2}\mathrm{tr}[\hat{F}]. \tag{17a}$$

The trace is explicitly expressed as follows:

$$\mathrm{tr}[\hat{F}]=[f_{11}^{(BA)}f_{22}^{(BA)}\{\exp(ik_{Tz}^{(A)}D_A+ik_{Tz}^{(B)}D_B)+\exp(ik_{Lz}^{(A)}D_A+ik_{Lz}^{(B)}D_B)\} -f_{12}^{(BA)}f_{21}^{(BA)}\{\exp(ik_{Tz}^{(A)}D_A+ik_{Lz}^{(B)}D_B)+\exp(ik_{Lz}^{(A)}D_A+ik_{Tz}^{(B)}D_B)\}] /(f_{11}^{(BA)}f_{22}^{(BA)}-f_{12}^{(BA)}f_{21}^{(BA)}). \tag{17b}$$

We emphasize here that $f^{(jk)}$ does not depend on n. The frequency of phonons are set to satisfies the resonant condition of transmission at SL2, i.e.

$$k_{Tz}^{(A)}D_A+k_{Tz}^{(B)}D_B =k_{Lz}^{(A)}D_A+k_{Lz}^{(B)}D_B+2\pi\ell\equiv\chi, \tag{18}$$

where ℓ is an integer. With this condition, Eqs. (16) and (17) have a following relation:

$$\tau=\frac{1}{2}\mathrm{tr}[\hat{F}]=e^{i\chi}\varepsilon_0, \tag{19a}$$

$$\varepsilon_0=\frac{f_{11}^{(BA)}f_{22}^{(BA)}-f_{12}^{(BA)}f_{21}^{(BA)}\cos\psi}{f_{11}^{(BA)}f_{22}^{(BA)}-f_{12}^{(BA)}f_{21}^{(BA)}}, \tag{19b}$$

where $\psi=k_{Tz}^{(A)}D_A-k_{Lz}^{(A)}D_A$ or $\psi=k_{Lz}^{(B)}D_B-k_{Tz}^{(B)}D_B$ because of Eq.(18). We note here that ε_0 is real and positive.[8] The facter $e^{i\chi}$ is either $+\delta^{1/2}$ or $-\delta^{1/2}$. The sign is determined by the value of χ in Eq.(18).

Analytic solution of Eq.(15) is

$$a_n=\frac{e^{i\alpha n}}{\sinh\theta}\{-a_0\sinh(n-1)\theta+a_1e^{-i\alpha}\sinh n\theta\}, \tag{20}$$

where

$$\cosh\theta = \tau/\delta^{1/2} \equiv \varepsilon \ , \tag{21}$$

$$2\alpha = (k_{Tz}^{(A)} + k_{Lz}^{(A)})D_A + (k_{Tz}^{(B)} + k_{Lz}^{(B)})D_B, \tag{22}$$

and; a_0 and a_1 are initial values of a_n at $n = 0$ and 1, respectively. At the resonant condition, $\varepsilon \equiv \pm\, \varepsilon_0$ and $\varepsilon_0 < 1$. Therefore:

$$\mathrm{Re}[\theta] = 0 \ , \tag{23a}$$

$$\mathrm{Im}[\theta] = \cos^{-1}|\varepsilon| = \cos^{-1}|\tau| . \tag{23b}$$

A period of oscillation of the transmission rate, p, is determined by Eq.(23b) as follows:

$$p = \frac{\pi}{\cos^{-1}|\varepsilon|} = \frac{\pi}{\cos^{-1}|\tau|} . \tag{24}$$

We find that Eq. (20) is able to reproduce characteristic features of the transmission rates similar to those calculated with the 4×4 transfer matrix. The validity of the present approximation can be seen in Fig.3, which compares the phonon transmission rates calculated exactly with the 4×4 transfer matrix (open circles) and the ones calculated with the 2×2 transfer matrix (solid lines).

Ⅳ. STRUCTURE OF THE MODE CONVERTER

The basic idea of a mode converter or selector is constructed in this section based on the above discussion.

In the Fig.3 (a), transmission/conversion rate from L mode to T mode is displayed for SL1 ($D_A = D_B = 3.6$nm, frequency ν_0 and incident angle $\phi^{(B)} = 45°$). In this case the resonant condition is not satisfied. However we can see an oscillation with a small amplitude. Period of the oscillation is $p_1 = 7.4$ BLs.

The resonant condition of transmission is satisfied in SL2 with the same condition as in Fig.3 (a) except the thickness, i.e., $D_A = D_B = 4.0$nm. The transmission/conversion rate oscillates with a period $p_2 = 11$ BLs and an amplitude is almost unity. That implies the energy of the L and T modes exchanges totally between them, and interaction with those modes is strong.

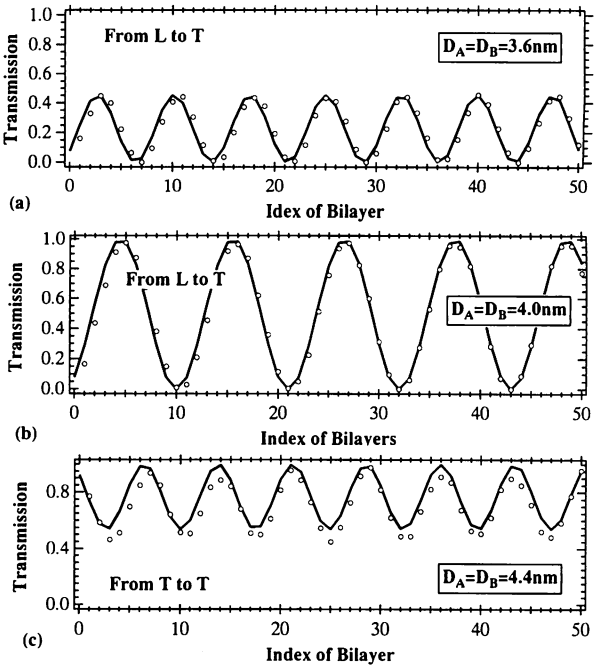

Fig.3. Transmission rate versus index of BL in a periodic GaAs/AlAs superlattice. Open circles are data calculated from the precise 4×4 matrices. Solid lines are given by the solution of the finite difference equations. (a) For the SL1, Incident L-mode phonons converted to T mode. However, the transmitted energy oscillates with distance of propagation with rather small amplitude. (b) In SL2, the same oscillation appears with a maximum amplitude,i.e. almost unity. (c) If the T-mode phonons are incident to SL3, the oscillation of T mode energy keeps a transmission rate at the top of the graph or near unity.

If we write down Eq. (20) for $a_0 = 0$, we can see that the strength of interaction between those modes have relation to the amplitude of oscillation. Energy is proportional to $|a_n|^2$, i.e.

$$|a_n|^2 = |a_1|^2 \left| \frac{\sinh n\theta}{\sinh \theta} \right|^2 , \tag{25}$$

where $a_1 \propto \hat{F}_{12}$ for pure L mode incidence .

The SL3 has thickness $D_A = D_B = 4.4$nm. With the same condition in Fig.3 (a) or (b) except the thickness of BLs, SL3 can keep the energy almost in T mode as in Fig.3 (c). However, the transmission rate also oscillates like (a) and (b) with a period $p_3 = 7.2$ BLs.

If we consider L mode incidence only from the substrate, the structure of a mode converter is designed as follows: Incident L mode phonons must be input to the SL2 without mode conversion. Therefore, the number of the BLs in SL1 is

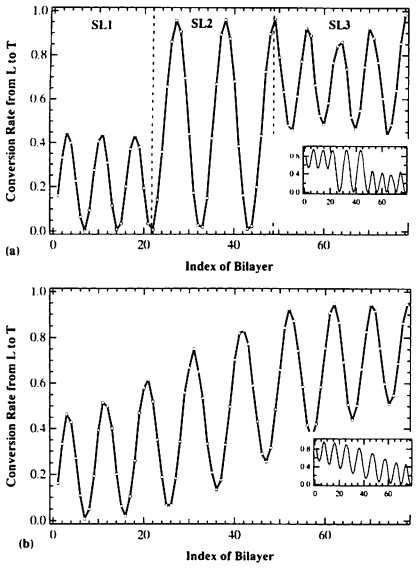

Fig.4. Transmission rate of transverse (T) phonons versus index of BL for longitudinal (L) phonon incidence (the angle of incidence in the substrate is 45° and the frequency is $\nu_0 = 812$GHz). (a) The transmission rate of T phonons or conversion rate from incident L phonons to T phonons is realized by the SL in Fig.1. (Inset is conversion from mode T to L.) (b) The conversion of phonon modes also takes place in the CHIRP superlattices more efficiently than the SL in Fig.1. However the thickness of each BL may bear a problem. (See text.)

took as mp_1 (m: an integer). We took m as 3 (i.e. # BLs = 22). If the incident phonons are mixed with both L and T modes, we can convert them by changing the number of BLs in SL1. The phonons can be put directly to SL2, but SL1 can change the incident phonons to pure L mode faster than SL2. In SL2, the mode conversion is completed with number of $(m + 1/2)\,p_2$ BLs. We put m as 2 (i.e. # BLs = 27). The SL3 keeps the mode in T. Therefore, number of BLs is not essential in this mode converter. However, to take the pure T mode we put the number of BLs as mp_3. We took as $m = 4$ (i.e. # BLs = 29). Therefore the whole structure of the SL have become as in Fig.1. We can see that the incident L-mode phonons are converted totally to T mode with the SL designed in the above discussion as in Fig.4(a).

If the thickness of layers in a SL is made thicker, the frequency of the dispersion relation is decreased. This is because the frequency is inversely proportional to the layer thickness. In Fig.2 and Fig.5(a), ν_1 expresses an equivalent frequency in SL2 assuming that the phonons in SL1 is moved into SL2. The frequency ν_2 is an equivalent frequency of phonons in SL2 if the phonons in SL3 are in SL2. The period of oscillation in Fig.4(a) is long in SL2 where the resonant condition is satisfied. In SL1 and SL3, it is short. If the frequency of the incident phonons slightly shifts to high region, the period of oscillation in SL1 becomes longer because the shifted frequency approaches the resonant frequency of SL1. If the incident frequency slightly shifts to low region, the oscillation period of SL3 becomes longer. In both cases, SL2 and the sub-SL at the opposit side have short periods. From this effect, we can expect that the SL with the three sub-SL's in Fig.1 can convert mode more efficiently than a SL only with SL2.

If the step of thickness, 0.8nm, of the single-layers (from 3.6nm in SL1 to 4.4nm in SL3) could be spread to each single layers (i.e. the thickness changes gradually by $0.8/78 \approx 0.010$ nm), such a SL would act as ideal mode converter as in Fig.4(b). That SL is called as a CHIRP superlattice. However it cannot be realized because the increased thickness is too small or less than an atomic size. If the layers could be fabricated much thicker, the mode converter could be more efficient. In this case, the frequency of the resonant condition becomes very low.

V. NUMERICAL RESULTS OF MODE CONVERSION

In fabricating the mode converter with the SL in Fig.1, we have to consider the incident phonons as a wave packet for real applications. Because the mode converter acts like a passive filter in electronics, we are allowed not to be nervous about the response speed. Therefore we consider continuous wave (CW) packets that are incident to the SL continuously in any time. Frequency distribution of the amplitude in the wave packet is assumed in the substrate as follows:

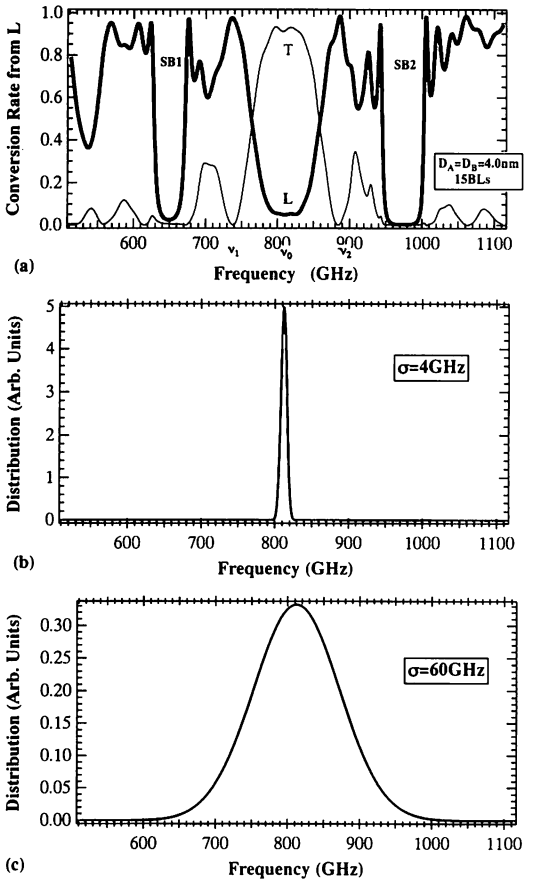

Fig.5. (a) Conversion rate from mode L to T and transmission rate of mode L in SL2 at 15th BL. Labels SB1 and SB2 correspond to the stop bands in the dispersion relation in Fig.2. Frequency distribution of incident wave packets to the SL is compared with the conversion rate: frequency widths are (b) σ =4GHz and (c) σ =60GHz.

$$a_L^{(S)}(\nu)\,\mathrm{d}\nu = \frac{1}{\sqrt{2\pi}\sigma}\exp\left[-\frac{(\nu-\nu_0)^2}{2\sigma^2}\right]\mathrm{d}\nu\,, \quad (26)$$

After the wave packet gets through the BLs, the amplitude is calculated by

$$a_{J,n}^{(j)}(x) = \int a_L^{(S)}(\nu)\,\gamma_{LJ,n}^{(j)}\,\mathrm{e}^{ik_{\parallel}x}\,\mathrm{d}\nu\,. \quad (27)$$

where n is the index of BL; $\gamma_{LJ,n}^{(j)}$ is a transmission/conversion rate from mode L to mode J (= L and T) from the substrate to the single-layer j in the BL n, and it is given by making use of the 4 × 4 matrices in Eq.(3). We note that $\gamma_{LJ,n}^{(j)}$ and $k_{\parallel}$ depend on the frequency ν. The intensity of the wave packet at BL n is directly proportional to $|a_{J,n}^{(j)}(x)|^2$.

The conversion/transmission rates from L mode to T/L are depicted in Fig.5 (a) for the SL2 with 15 BLs. Here we consider two CW packets. One is with a narrow frequency width σ = 4GHz as in Fig.5(b), and the other is with a broad frequency width σ = 60GHz as in Fig.5 (c). The width of the packet in the real space along the x direction is inversely proportional to the frequency width σ. Along the z direction the packet have the same intensity. We show how the packets propagate through the SL in Fig.6. From the top to the bottom, there are depicted the incident packet, packets out of SL1 getting into SL2, packets out of SL2 getting into

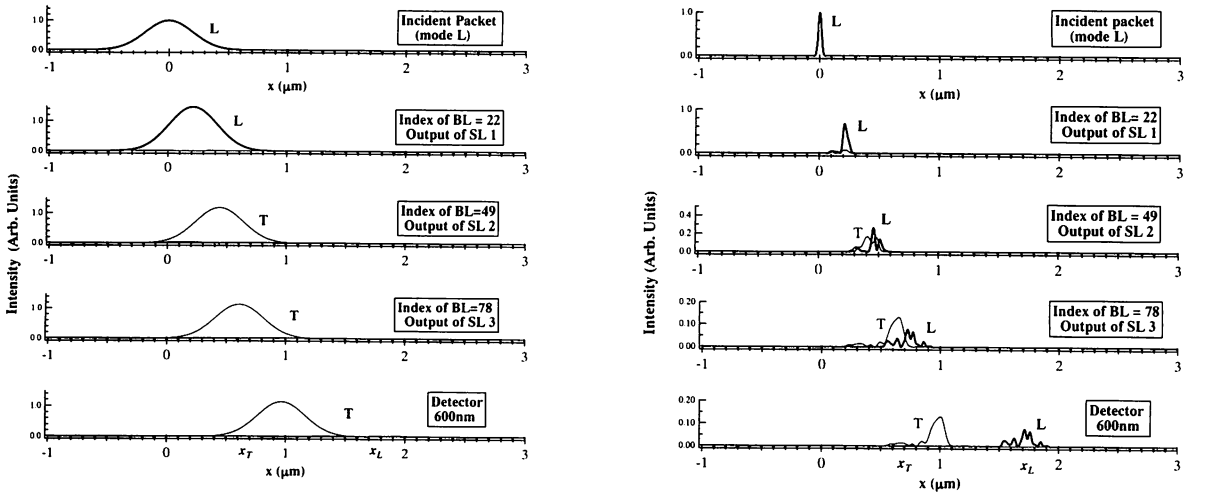

Fig.6. Propagation of the wave packet is depicted at the input (incidence) of SL1, the output of SL1, the output of SL2, the output of SL3, and detector after 600nm depart from the output of SL3. The widths of wave packet in the real space are inversely proportional to the frequency widths: (a) With σ =4GHz the SL acts as a mode converter. (b) With σ =60GHz, the SL plays a role of a mode selector.

SL3, packets out of SL3 getting into the detector layer with a 600nm buffering region, and packets in the detector.

Figure 6 (a) is for σ = 4GHz. The incident CW packet with pure L mode is totally converted to T mode with a broad width in the real space. The SL acts as a mode converter with precise accuracy.

Figure 6 (b) is for σ = 60GHz. Because the frequency distribution of the packet is broad as in Fig.5 (b), the incident CW packet of pure L mode cannot be converted T mode. Therefore, the wave packets appeared in the detector have two peaks with different modes L and T. However they are separated enough from each other because the width in real space is narrow. Further the packet of mode T in the detector have a peak with a frequency width, σ, about 20GHz. This is a width of frequencies in Fig.5 (a) where the mode conversion have the highest efficiency around the resonant frequency ν_0. Thus the SL acts as both a mode selector and a frequency filter in this situation.

If we assume that a plane wave of mode L are propagating through the SL without mode conversions, the location where the wave should appear in the detector can be predicted as x_L = 1753nm by the method of geometrical optics. If we treat a L mode plane wave, the location should be x_T = 687nm with the same method. In the case of the CW packets with the mode conversion, they appear in a range from x_T to x_L. We can see this feature in Fig.6.

Ⅵ. SUMMARY

In this article we have shown that the transfer matrix method is also useful to analyze the resonant condition of transmission. The 2 × 2 matrices is introduced near the frequencies of the resonant condition and they are reduced to the finite deference equations, and they are solved analytically.

Based on the above discussions, a structure of the mode converter is proposed. The structure is similar to the CHIRP superlattice in device applications, and the mechanism of the mode conversion is analogous to the MSW effect in the field of neutrino physics, but not homogeneous. The mode conversion in Fig.4 (a) is of the nonadiabatic process while the process in Fig.4 (b) is adiabatic.

The CHIRP superlattice has an efficiency to convert the phonon mode. However, the frequency of the incident phonons should be extremely low. To construct the mode converter for high frequency phonons we have to make use of the oscillations of transmission /conversion rates near the frequency of the resonant condition of transmission. Further, we show this SL works also as a mode selector.

References

[1] H. Kato, H. J. Maris, S. Tamura, Phys. Rev. B53, 7884 (1996) ; Physica B 219 & 220, 696 (1996).

[2] A. Howie and M. J. Whelan, Proc. Roy. Soc. A263, 217 (1961).

[3] N. Kato, Acta Cryst. 16, 276 (1963) ; 14, 526 (1961) . B.E. Warren, p.339, *X-ray Diffraction* (Addson-Wesley 1969).

[4] L. Wolfenstein, Phys. Rev. D17, 2369 (1978) ; D20, 2634 (1979).

[5] S. P. Mikheyev and A. Y. Smirnov, Sov. J. Nucl. Phys. 42, 913 (1986); Sov. Phys. JETP 64, 4 (1986).

[6] T. Nakagawa, N. J. Kawai, K. Ohta, M. Kawashima, Electron. Lett. 19, 822 (1983).

[7] H. Kato, J. Acoust. Soc. Am., in press by April in 1997.

[8] H. Kato, S. Tamura, J. Phys. C, to be published.